11 Scale setting

Authors: R. Sommer, N. Tantalo, U. Wenger

Matching QCD to Nature requires fixing the quark masses and matching an overall scale to experiment. That overall energy scale $\mathcal{S}$ may be taken, for example, as the nucleon mass. This process is referred to as scale setting.

11.1 Impact

The scale setting procedure, described in some detail below, is a rather technical step necessary to obtain predictions from QCD. What may easily be overlooked is that the exact predictions obtained may depend rather sensitively on the scale.

As long as the theory is incomplete, e.g., because we have predictions from $N_f = 2 + 1$ QCD, results will depend on which physics scale is used. Whenever a theory scale (see Sec. 11.5) is used, it matters which value one imposes. Thus, to know whether computations of a particular quantity agree or not, one should check which (value for a) scale was used.

The sensitivity of predictions to the scale vary with the observable. For example, the Λ parameter of the theory has a linear dependence,

$$\frac{\delta\Lambda}{\Lambda} \approx \frac{\delta\mathcal{S}}{\mathcal{S}}\,, \tag{460}$$

because Λ has mass dimension one and other hidden dependences on the scale are (usually) suppressed. Let us preview the results. The present precision on the most popular theory scale, w_0 in Eq. (510) is about 0.4% and for $\sqrt{t_0}$ it is 0.6%. On the Λ parameter it is about 3%. Thus, we would think that the scale uncertainty is irrelevant. However, in Sec. 11.8 we will discuss that differences between $N_f = 2 + 1$ and 2+1+1 numbers for $\sqrt{t_0}$ are at around 2% which *does matter*.

Also, light-quark masses have an approximatively linear dependence on the scale (roughly speaking one determines, e.g., $m_{ud} = \frac{1}{\mathcal{S}} \times [m_\pi^2]_{\rm exp} \times [\frac{m_{ud}\mathcal{S}}{m_\pi^2}]_{\rm lat}$) and scale uncertainties may play an important rôle in the discussion of agreement vs. disagreement of computations within their error budget.

The list of quantities where scale setting is very important may be continued; we just want to mention an observable very much discussed at present, the hadronic vacuum polarisation contribution to the anomalous magnetic moment of the muon [1]. It is easily seen that the dependence on the scale is about quadratic in that case [2],

$$\frac{\delta a_\mu^{\rm HVP}}{a_\mu^{\rm HVP}} \approx 2\frac{\delta\mathcal{S}}{\mathcal{S}}\,. \tag{461}$$

This fact means that scale setting has to be precise at the few per-mille precision to have an impact [3] on the discussion whether or not a_μ computed in the standard model shows a deviation from experiment.

11.2 Scale setting as part of hadronic renormalization schemes

We consider QCD with N_f quarks and without a θ-parameter. This theory is completely defined by its coupling constant as well as N_f quark masses. After these parameters are

specified all other properties of the theory are predictions. Coupling and quark masses depend on a renormalization scale μ as well as on a renormalization scheme. The most popular scheme in the framework of perturbative computations is the $\overline{\rm MS}$ scheme, but one may also define nonperturbative renormalization schemes, see Secs. 3 and 9.

In principle, a lattice computation may, therefore, use these N_f+1 parameters as input together with the renormalization scale μ to fix the bare quark masses and coupling of the discretized Lagrangian, perform continuum and infinite volume limit and obtain desired results, e.g., for decay rates.[1] However, there are various reasons why this strategy is inefficient. The most relevant one is that coupling and quark masses cannot be obtained from experiments without invoking perturbation theory and thus necessarily truncation errors. Moreover, these parameters are naturally short distance quantities, since this is where perturbation theory applies. Lattice QCD on the other hand is most effective at long distances, where the lattice spacing plays a minor role. Therefore, it is more natural to proceed differently.

Namely, we may fix N_f+1 nonperturbative, long-distance observables to have the values found in Nature. An obvious choice are N_f+1 hadron masses that are stable in the absence of weak interactions. This hadronic renormalization scheme is defined by

$$\frac{M_i(g_0,\{am_{0,\mathrm{j}}\})}{M_1(g_0,\{am_{0,\mathrm{j}}\})} = \frac{M_i^{\rm exp}}{M_1^{\rm exp}}\,, \quad i=2\ldots N_f+1\,, \quad j=1\ldots N_f\,. \tag{462}$$

Here, M_i are the chosen hadron masses, g_0 is the bare coupling, and $am_{0,j}$ are the bare quark masses in lattice units. The ratio M_i/M_1 is, precisely speaking, defined through the hadron masses in lattice units, but in infinite volume. In QCD (without QED), all particles are massive. Therefore, the infinite volume limit of the properties of stable particles is approached with exponentially small corrections which are assumed to be estimated reliably. The power-like finite-volume corrections in QCD+QED are discussed in subsection 11.3. For fixed g_0, Eq. (462) needs to be solved for the bare quark masses,

$$am_{0,\mathrm{j}} = \mu_j(g_0)\,. \tag{463}$$

The functions μ_j define a line in the bare parameter space, called the line of constant physics. Its dependence on the set of masses $\{M_i\}$ is suppressed. The continuum limit is obtained as $g_0\to 0$ with the lattice spacing shrinking roughly as $aM_1\sim \mathrm{e}^{-1/(2b_0g_0^2)}$. More precisely, consider observables $\mathcal{O}$ with mass dimension $d_{\mathcal{O}}$. One defines their dimensionless ratio

$$\hat{\mathcal{O}}(aM_1) = \left.\frac{\mathcal{O}}{M_1^{d_{\mathcal{O}}}}\right|_{am_{0,j}=\mu_j(g_0)}\,, \tag{464}$$

and obtains the continuum prediction as

$$\mathcal{O}^{\rm cont} = (M_1^{\rm exp})^{d_{\mathcal{O}}} \lim_{aM_1\to 0}\hat{\mathcal{O}}(aM_1) \tag{465}$$

which explains why the determination and use of aM_1 is referred to as scale setting.

Equation (463) has to be obtained from numerical results. Therefore, it is easiest and most transparent if the i-th mass ratio depends predominantly on the i-th quark mass. Remaining for a while in the isospin-symmetric theory with $m_{0,1}=m_{0,2}$ (we enumerate the quark masses

[1] At first sight this seems like too many inputs, but note that it is the scale μ, at which $\alpha(\mu)$ has a particular value, which is the input. The coupling α by itself can have any (small) value as it runs.

in the order up, down, strange, charm, bottom and ignore the top quark), we have natural candidates for the numerators as the pseudoscalar masses in the associated flavour sectors, i.e., π, K, D, B. The desired strong dependence on light- (strange-)quark masses of π- (K-)meson masses derives from their pseudo-Goldstone nature of the approximate $SU(3)_{\rm L} \times SU(3)_{\rm R}$ symmetry of the massless QCD Lagrangian which predicts that M_π^2 is roughly proportional to the light-quark mass and $M_{\rm K}^2$ to the sum of light- and strange-quark masses. For D and B mesons approximate heavy-quark symmetry predicts M_D and M_B to be proportional to charm- and bottom-quark masses. Also other heavy-light bound states have this property. There is another important feature which singles out pseudoscalar masses. Because they are the lightest particles with the given flavour quantum numbers, their correlation functions have the least signal/noise problem in the Monte Carlo evaluation of the path integral [4, 5].

Still restricting ourselves to isospin-symmetric QCD (isoQCD), we thus take it for granted that the choice M_i, $i \geq 2$ is easy, and we do not need to discuss it in detail: the pseudoscalar meson masses are very good choices, and some variations for heavy quarks may provide further improvements.

The choice of M_1 is more difficult. From the point of view of physics, a natural choice is the nucleon mass, $M_1 = M_{\rm nucl}$. Unfortunately it has a rather bad signal/noise problem when quark masses are close to their physical values. The ratio of signal to noise of the correlation function at time x_0 from N measurements behaves as [4]

$$R_{S/N}^{\rm nucl} \overset{x_0 \text{ large}}{\sim} \sqrt{N}\, \exp(-(m_{\rm nucl} - \frac{3}{2} m_\pi)\, x_0) \approx \sqrt{N}\, \exp(-x_0/0.27\,\text{fm})\,, \tag{466}$$

where the numerical value of 0.27 fm uses the experimental masses. The behaviour in practice, but at still favourably large quark masses, is illustrated in Fig. 50. Because this property leads to large statistical errors and it is further difficult to control excited-state contaminations when statistical errors are large, it is useful to search for alternative physics scales. The community has gone this way, and we discuss some of them below. For illustration, here we just give one example: the decay constants of leptonic π or K decays have mass dimension one and can directly replace M_1 above. Figure 50 demonstrates their long and precise plateaux as a function of the Euclidean time. Advantages and disadvantages of this choice and others are discussed more systematically in Sec. 11.4.

11.2.1 Theory scales

Since the signal/noise problem of physics scales is rather severe, they were already replaced by theory scales in the very first days of lattice QCD. These scales cannot be determined from experiment alone. Rather, their values have to be computed by lattice QCD using a physics scale as input.

Creutz already used the string tension in his seminal paper on $SU(2)$ Yang Mills theory [11], because it is by far easier to determine than glueball masses. A further step was made by the potential scale r_0, defined in terms of the static force $F(r)$ as [12]

$$r_0^2 F(r_0) = 1.65\,. \tag{467}$$

Even though r_0 can vaguely be related to the phenomenology of charmonium and bottomonium states, its precise definition is in terms of $F(r)$ which can be obtained accurately from Monte Carlo lattice computations with (improvable) control over the uncertainties, but not from experiment. In that sense, it is a prototype of a theory scale.

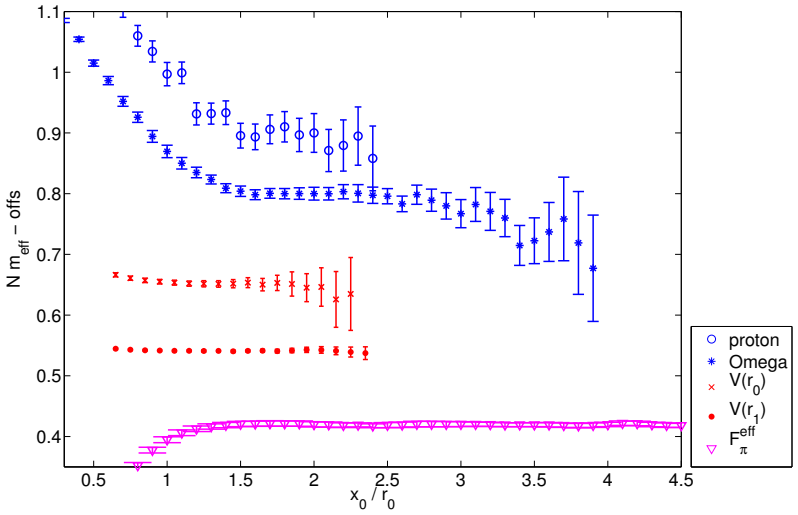

Figure 50: Effective masses for M_{proton} [6], M_Ω [7], $V(\approx r_0)$, $V(\approx r_1)$ [8] and f_π [9] on $N_f = 2$ CLS ensemble N6 with $a = 0.045\,\text{fm}, M_\pi = 340$ MeV on a $48^3\,96$ lattice [9]. All effective "masses" have been scaled such that the errors in the graph reflect directly the errors of the determined scales. They are shifted vertically by arbitrary amounts. Figure from Ref. [10]. Note that this example is at still favourably large quark masses. The situation for M_{proton} becomes worse closer to the physical point, but may be changed by algorithmic improvements.

Useful properties of a good theory scale are high statistical accuracy, easy to control systematics (also large volume), quark mass dependence only due to the fermion determinant, and low numerical cost for its evaluation. These properties are realized to varying degrees by the different theory scales covered in this section and, in this respect, they are much preferred compared to physics scales. Consequently, the physics scale M_1 has often been replaced by a theory scale as, e.g., $\mathcal{S} = r_0^{-1}$ in the form

$$\mathcal{O}^{\text{cont}} = \left(\mathcal{S}^{\text{phys}}\right)^{d_\mathcal{O}} \lim_{a\mathcal{S}\to 0} \hat{\mathcal{O}}_\mathcal{S}(a\mathcal{S}) \quad \text{with} \quad \hat{\mathcal{O}}_\mathcal{S}(a\mathcal{S}) = \left[\mathcal{S}^{-d_\mathcal{O}}\,\mathcal{O}\right]_{am_{0,j}=\mu_j(g_0)}\,, \tag{468}$$

and

$$\mathcal{S}^{\text{phys}} = (M_1^{\text{exp}}) \lim_{aM_1\to 0} \hat{\mathcal{S}}_{M_1}(aM_1)\,. \tag{469}$$

In this section, we review the determination of numerical results for the values of various theory scales in physical units, Eq. (469). The main difficulty is that a physics scale M_1 has to be determined first in order to connect to Nature and, in particular, that the continuum limit of the theory scale in units of the physics scale has to be taken.

11.3 Isospin breaking, electromagnetism, and definition of hadronic schemes

11.3.1 The approximate nature of QCD

For simplicity and because it is a very good approximation, we have assumed above that all other interactions except for QCD can be ignored when hadron masses and many other

properties of hadrons are considered. This is a natural point of view because QCD is a renormalizable field theory and thus provides unique results.

However, we must be aware that while it is true that the predictions (e.g., for hadron masses M_i, $i > N_f + 1$) are unique once Eq. (462) is specified, they will change when we change the inputs $M_i^{\rm exp}$. These ambiguities are due to the neglected electroweak and gravitational interactions, namely because QCD is only an approximate—even if precise—theory of hadrons. At the sub-percent level, QED effects and isospin violations due to $m_u \neq m_d$ must be included. At that level one has a very precise description of Nature, where weak decays or weak effects, in general, can be included perturbatively and systematically in an effective field theory description through the weak effective interaction Hamiltonian, while gravity may be ignored.

We now discuss how to handle the scale setting as part of the renormalization of QCD+QED. Note that a similar discussion with emphasis on quark masses can be found in Sec. 3. In the following discussion, we focus more on the issues related to the scale setting (see also Ref. [13]). In this connection, triviality of QED does not play a rôle at small enough α: we may think of replacing the continuum limit $a \to 0$ by a limit $a \to a_{\rm w}$ with $a_{\rm w}$ nonzero but very far below all QCD+QED scales.

11.3.2 Hadronic renormalization of QCD+QED

The definition and implementation of a hadronic renormalization scheme of QCD+QED defined on the lattice needs some additions to subsection 11.2 which we now discuss.

In addition to the $N_f + 1$ parameters of the QCD action (without isospin symmetry), one now also has the elementary electric charge e. This requires $N_f + 2$ experimentally measurable observables to fix the bare parameters of the theory. A natural choice for the experimental inputs are again hadron masses. Indeed, hadron masses are infrared safe quantities also in QCD+QED, while in the cases of cross sections and decay rates, infrared divergences appear at intermediate stages of the calculations (see below). Therefore, we consider the generalization

$$\frac{M_i(g_0, e_0, \{am_{0,\rm j}\})}{M_1(g_0, e_0, \{am_{0,\rm j}\})} = \frac{M_i^{\rm exp}}{M_1^{\rm exp}}\,, \quad i = 2 \ldots N_f + 2\,, \quad j = 1 \ldots N_f \tag{470}$$

of Eq. (462). Here, M_i are the chosen hadron masses, g_0 the bare strong coupling, e_0 the bare electric charge, and $am_{0,j}$ are the bare quark masses in lattice units. For fixed g_0, the system of equations (470) now needs to be solved for the bare quark masses and the bare electric charge,

$$am_{0,\rm j} = \mu_j(g_0)\,, \qquad e_0 = {\rm e}(g_0)\,, \tag{471}$$

to obtain the line of constant physics of the theory. Some observations are in order.

So far, we have assumed that QCD+QED is simulated nonperturbatively in the electromagnetic coupling constant $\alpha_{\rm em}$. In this case, the bare electric charge can be conveniently fixed by considering among the experimental inputs both the charged and neutral pion masses. Indeed, by neglecting terms of $\mathcal{O}((m_u - m_d)^2)$ [14] one has that $m_{\pi^+}^2 - m_{\pi^0}^2 \sim \alpha_{\rm em}$. If the theory is instead treated neglecting $\mathcal{O}(\alpha_{\rm em}^2)$ contributions, the electric charge does not renormalize and it is consistent and convenient to fix it by the condition [15]

$$\frac{4\pi}{e_0^2} = \frac{1}{\alpha_{\rm em}^{\rm Thomson}} = 137.035999084(21)\,. \tag{472}$$

Another important difference from pure QCD concerns finite-volume effects. In contrast to the exponentially suppressed finite-volume effects of stable hadron masses at $\alpha_{\rm em} = 0$, in QCD+QED with $\alpha_{\rm em} > 0$ finite-volume effects are

$$\frac{M_i(g_0, e_0, am_{0,\rm j}; L)}{M_i(g_0, e_0, am_{0,\rm j}; \infty)} = 1 + \frac{\alpha_{\rm em} q_i^2 \xi(1)}{L M_i(g_0, e_0, am_{0,\rm j}; \infty)} + \frac{\alpha_{\rm em} q_i^2 \xi(2)}{[L M_i(g_0, e_0, am_{0,\rm j}; \infty)]^2} + O\left(L^{-n}, \alpha_{\rm em}^2\right) , \tag{473}$$

where q_i is the electric charge of the hadron in units of the charge of the positron, the $\xi(i)$ are known numerical constants that depend on the spatial boundary conditions, and the remainder terms start with a power $n = 3$ in the $\mathrm{QED_L}$ formulation[16, 17] and with $n = 4$ in $\mathrm{QED_C}$ [18]. These two definitions of QED in a finite volume are discussed in Refs. [19–21] and Refs. [18, 22, 23], respectively. For other formulations [24–26], we refer to Sec. 3 and for a discussion on open problems to Ref. [27]. Since the bare parameters need to be fixed through experimental observables, finite volume effects have to be removed from the M_i and the behaviour Eq. (473) is crucial in this respect.

Another important observation concerns the use of observables associated with decay rates or cross sections in setting the scale. The issue is particularly subtle in QCD+QED because of the well known problem associated with the appearance of infrared divergences at intermediate stages of the calculations. The solution requires a proper definition of infrared-safe observables, according to the Bloch–Nordsieck mechanism [28]. These measurable observables are obtained by including in the final state of a process any number of soft photons with total energy up to a given physical threshold. Once the infrared-safe measurable observable has been constructed, it can be used in the scale setting as any other measurable quantity. A particularly relevant example is the leptonic decay rate of the pion,

$$\Gamma^{\rm QCD+QED}[\pi^- \mapsto \mu \bar{\nu}_\mu(\gamma), E_\gamma] \, . \tag{474}$$

Here, phase space is integrated over with the constraint that the total energy of the photons is below E_γ. The feasibility of using such an observable in place of a stable hadron mass has to be judged on the basis of the overall precision, statistical plus systematics, that is achievable in the lattice calculation (see Refs. [13, 29]).

11.3.3 Hadronic definition of QCD and of QED corrections

Under the assumption of negligible weak (and gravity) corrections QCD+QED is the complete theory and, therefore, the predictions obtained from lattice simulations for any observable $\mathcal{O}^{\rm QCD+QED}$, that has not already been used in the scale setting, are unambiguous. On the contrary, what we call the QCD contribution $\mathcal{O}^{\rm QCD}$ and the associated radiative corrections,

$$\delta\mathcal{O}^{\rm QCD} = \frac{\mathcal{O}^{\rm QCD+QED}}{\mathcal{O}^{\rm QCD}} - 1 \, , \tag{475}$$

do depend upon the inputs used to define QCD.

Going back to Eq. (462), different hadronic definitions of QCD can be obtained by chosing different hadron masses and/or different values for the "physical" inputs. Once we have chosen which hadron masses to use, the different hadronic schemes can be identified by writing

$$\frac{M_i(g_0, \{am_{0,\rm j}\})}{M_1(g_0, \{am_{0,\rm j}\})} = \frac{M_i^{\rm QCD}}{M_1^{\rm QCD}} \, , \quad i = 2 \ldots N_f + 1 \, , \quad j = 1 \ldots N_f \, , \tag{476}$$

and by specifying the values of the external inputs, for example parameterized by $\varepsilon_i^{\rm QCD}$ in[2]

$$M_i^{\rm QCD} = M_i^{\rm exp}\left(1+\varepsilon_i^{\rm QCD}\right) . \tag{477}$$

A "natural" choice is to set $\varepsilon_i^{\rm QCD}=0$, i.e., to define QCD by using exactly the experimental values for the stable hadron masses entering the calibration procedure. In this case, if the same hadron mass is used in the definition of the full theory, Eq. (470), and in the definition of QCD, then the radiative corrections on these quantities are zero by construction. Radiative corrections on any other predictable quantity are well defined and nonvanishing.

In light of this observation, the introduction of the $\varepsilon_i^{\rm QCD}$ parameters might appear unnecessary. However, this is not the case for the following reasons. Isosymmetric QCD (isoQCD), already introduced in Sec. 11.2, is another good approximation of the real world. Due to $m_u = m_d = m_{ud}$, the theory only depends on N_f parameters. In order to set the masses of the light and strange quarks in isoQCD the options of using the charged or the neutral pion and kaon masses are equally valid from the physical point of view. If one picks, e.g., the neutral meson masses, then one has nonzero ε_i when the right hand side of Eq. (477) is written in terms of the charged ones. Furthermore, on the basis of symmetry arguments and/or (chiral) effective theory calculations one may argue that certain linear combinations of charged and neutral meson masses are more "natural" than others (see the discussion in the quark-mass section, Sec. 3) because the resulting radiative corrections are smaller.

As a matter of fact, many of the existing lattice calculations have been performed in the isospin-symmetric limit, but not all the results considered in this review correspond to the very same definition of QCD. The commonly adopted values for the pion and Ω masses in isoQCD are

$$M_\pi^{\rm isoQCD} = M_{\pi^0}^{\rm exp}\,, \qquad M_\Omega^{\rm isoQCD} = M_{\Omega^-}^{\rm exp} \quad \text{in Refs. [31–33]}\,.$$

For the kaon mass in isoQCD different collaborations made different choices, e.g., the values

$$\begin{aligned} M_K^{\rm isoQCD} &= 494.2(4)\ \text{MeV} \quad \text{in Refs. [31, 34, 35]}\,, \\ M_K^{\rm isoQCD} &= 495.7\ \text{MeV} \quad \text{in Ref. [32]}\,, \\ M_K^{\rm isoQCD} &= 497.6\ \text{MeV} \quad \text{in Ref. [33]}\,. \end{aligned}$$

The different choices of experimental inputs are perfectly legitimate if QED radiative corrections are neglected, but in principle predictions of isoQCD do depend on these choices, and it is not meaningful to average numbers obtained with different inputs. However, at the present level of precision the sub-percent differences in the inputs are most likely not relevant, and we will average and compare isoQCD results irrespective of these differences. The issue will become important when results become significantly more precise. Of course, it may not be ignored, when radiative corrections, Eq. (475), are directly compared between collaborations. In this case, we strongly suggest to compare results for the unambiguous full theory observable or to stick to a standard.

[2] After having calibrated the full theory (QCD+QED) with physical hadronic inputs, one can compute the strong coupling constant and the quark masses in a given renormalization scheme. These can then be used to define QCD by matching the corresponding renormalized quantities. This is the so–called GRS approach originally introduced in Ref. [30]. We refer to Ref. [13] for a discussion concerning the connection of the ε–language used here and the GRS scheme, and to Sec. 3 for a detailed discussion of the different schemes that have been used in the literature to define (iso)QCD including the original references on the subject.

Indeed, for the future, it is highly desirable to define such a standard for the parameters used to define (iso)QCD. We suggest using[3]

$$\begin{aligned} M_\pi^{\rm isoQCD} &= M_{\pi^0}^{\rm exp}\,, \\ M_K^{\rm isoQCD} &= M_{K^0}^{\rm exp}\,, \end{aligned} \tag{478}$$

while it is difficult to define a standard scale M_1 right now. Going by the majority of the large-scale computations, the two options m_Ω and pion leptonic decay rate are equally popular at the moment (see Sec. 11.4).

Since leptonic decay rates of pion and kaon play a prominent rôle in scale setting, we discuss the (pure) QCD definition of these quantities and of the associated radiative corrections in some detail. There are no ambiguities in the definition of the physical observable in QCD+QED that, in this case, is the decay rate introduced in Eq. (474) above. We now assume that (iso)QCD has been *already defined* by using as hadronic inputs hadron masses. It is then possible to compute the leptonic decay rate in QCD,

$$\Gamma^{\rm QCD}[\pi \mapsto \mu\bar\nu_\mu] = \frac{G_F^2}{8\pi}|V_{ud}|^2\, M_{\pi^-}^{\rm exp}\left(m_\mu^{\rm exp}\right)^2\left[1-\frac{\left(m_\mu^{\rm exp}\right)^2}{\left(M_{\pi^-}^{\rm exp}\right)^2}\right]\left(f_\pi^{\rm QCD}\right)^2 \tag{479}$$

where the so–called decay constant of the pion is given by

$$f_\pi^{\rm QCD} = \frac{\langle 0|\,\bar u\gamma^0\gamma^5 d\,|\pi\rangle^{\rm QCD}}{M_\pi^{\rm QCD}}\,. \tag{480}$$

Radiative corrections to $f_\pi^{\rm QCD}$ are then defined by

$$\delta f_\pi^{\rm QCD}(E_\gamma) = \sqrt{\frac{\Gamma^{\rm QCD+QED}[\pi^- \mapsto \mu\bar\nu_\mu(\gamma), E_\gamma]}{\Gamma^{\rm QCD}[\pi\mapsto\mu\bar\nu_\mu]}} - 1\,, \tag{481}$$

such that

$$\Gamma^{\rm QCD+QED}[\pi^- \mapsto \mu\bar\nu_\mu(\gamma), E_\gamma] = \Gamma^{\rm QCD}[\pi\mapsto\mu\bar\nu_\mu]\left[1+\delta f_\pi^{\rm QCD}(E_\gamma)\right]^2\,. \tag{482}$$

We want to stress once again that the definition of $\delta f_\pi^{\rm QCD}(E_\gamma)$ is not unique. As in the case of any other observable, different values of $\delta f_\pi^{\rm QCD}(E_\gamma)$ are obtained if one changes the prescription used to define QCD. In this case, in addition, one has to specify the photon energy treshold E_γ and, moreover, the exact expression used to define $\Gamma^{\rm QCD}$. Indeed, it would be perfectly legitimate to replace $M_{\pi^-}^{\rm exp}$ appearing in the kinematical factors of Eq. (479) with $M_\pi^{\rm QCD}$. The effect of such a different definition of $\Gamma^{\rm QCD}$ would be compensated by a change in $\delta f_\pi^{\rm QCD}(E_\gamma)$ with no ambiguities in the full theory observable $\Gamma^{\rm QCD+QED}$.

We mentioned in Sec. 11.2 that there are advantages from the numerical point of view in using the leptonic decay constants of the mesons in the QCD scale setting procedure.

[3] We note that the π^0 is unstable in QCD+QED and, therefore, it is much more convenient to use $M_{\pi^+}^{\rm exp}$ to calibrate the full theory. Although it is perfectly consistent to use different observables in the calibration of the full theory and of isoQCD, in the specific case one can write $M_\pi^{\rm isoQCD} = M_{\pi^+}^{\rm exp}(1+\varepsilon_\pi^{\rm isoQCD})$ with $\varepsilon_\pi^{\rm isoQCD} = (M_{\pi^0}^{\rm exp} - M_{\pi^+}^{\rm exp})/M_{\pi^+}^{\rm exp}$. In that language, the same observable is used in both theories but with a nonvanishing ε.

That observation can now be made more precise in light of the discussion of the previous paragraph. When we say that we use f_π to calibrate QCD, we mean that we choose a value for the $\delta f_\pi^{\rm QCD}(E_\gamma)$ and we *define*

$$f_\pi^{\rm QCD} = \frac{1}{1+\delta f_\pi^{\rm QCD}(E_\gamma)} \sqrt{\frac{\Gamma^{\rm exp}[\pi^- \mapsto \mu\bar{\nu}_\mu(\gamma), E_\gamma]}{\frac{G_F^2}{8\pi}|V_{ud}|^2\, M_{\pi^-}^{\rm exp}\, (m_\mu^{\rm exp})^2 \left[1-\frac{(m_\mu^{\rm exp})^2}{(M_{\pi^-}^{\rm exp})^2}\right]}}\,. \tag{483}$$

In the notation of the ε parameters introduced above, one has

$$1+\varepsilon_{f_\pi}^{\rm QCD} = \frac{1}{1+\delta f_\pi^{\rm QCD}(E_\gamma)}\,. \tag{484}$$

Again, a possible choice would be to set $\varepsilon_{f_\pi}^{\rm QCD}$ to zero and to use directly the experimentally measured decay rate at a given value of E_γ.[4] Common practice among the different lattice collaborations is to set

$$E_\gamma = E_\gamma^{\rm max} = \frac{M_{\pi^-}^{\rm exp}}{2}\left[1-\frac{(m_\mu^{\rm exp})^2}{(M_{\pi^-}^{\rm exp})^2}\right]\,, \tag{485}$$

the maximum energy allowed to a single photon in the case of negligible $\mathcal{O}(\alpha_{\rm em}^2)$ corrections, and to use the value

$$\delta f_\pi^{\rm isoQCD}(E_\gamma^{\rm max}) = 0.0088(11) \tag{486}$$

obtained in Refs. [36–38] in chiral perturbation theory and using the standard definition Eq. (478). The corresponding number for kaon decays is

$$\delta f_K^{\rm isoQCD}(E_\gamma^{\rm max}) = 0.0053(11)\,. \tag{487}$$

A recent lattice determination in the electro-quenched approximation [13]

$$\delta f_\pi^{\rm isoQCD}(E_\gamma^{\rm max}) \;=\; 0.0076(9)\,, \tag{488}$$

agrees well with Eq. (486), while the number for Kaon decays,

$$\delta f_K^{\rm isoQCD}(E_\gamma^{\rm max}) \;=\; 0.0012(5)\,, \tag{489}$$

differs by more than three (quadratically combined) error bars from Eq. (487). The scheme dependence can be neglected at the present level of accuracy.

11.4 Physical scales

The purpose of this short section is to summarize the most popular scales and give a short discussion of their advantages and disadvantages. We restrict ourselves to those used in more recent computations and thus have a rather short list.

[4] This procedure unavoidably requires that one provides a value for the CKM matrix element V_{ud} that has then to be considered an input of the lattice calculation and not a predictable quantity.

11.4.1 The mass of the Ω baryon

As already discussed, masses of hadrons that are stable in QCD+QED and have a small width, in general, are very good candidates for physical scales since there are no QED infrared divergences to be discussed. Furthermore, remaining within this class, the radiative corrections $\delta M_i^{\rm QCD}$, Eq. (475), are expected to be small. Furthermore, the Ω baryon has a significantly better noise/signal ratio than the nucleon (see Fig. 50). It also has little dependence on up- and down-quark masses, since it is composed entirely of strange valence quarks.

Still, one has to be aware that the mass is not extracted from the plateau region but from a modelling of the approach to a plateau in the form of fits [3, 31–33, 39, 40]. In this sense, the noise/signal ratio problem may persist. The use of various interpolating fields for the Ω helps in constraining such analyses, but it would be desirable to have a theoretical understanding of multi-hadron (or in QCD+QED multi-hadron + photon) contributions as it exists for the nucleon [41] as discussed in Sec. 10. In the present review, we take the estimates of the collaborations at face value and do not try to apply a rating or an estimate of systematic error due to excited-state contributions.

11.4.2 Pion and kaon leptonic decay rates

These decay rates have been discussed above. Here, we just summarize the main issues. In QCD+QED there is so far only one computation of the decay rate in the electro-quenched approximation [13]. The derived estimate for the radiative corrections agrees with the estimates from chiral perturbation theory (see Eqs. (486) and (487)). The quoted uncertainties are at the level of 0.001. This directly sets a limit to the achievable precision on the scale in isoQCD. At present, this limit is not yet relevant. A second source of uncertainty is due to the knowledge of V_{ud} and V_{us}. For convenience, we summarize the isoQCD values

$$f_\pi^{\rm isoQCD}\,|V_{ud}| = 127.13(2)_{\rm exp}(13)_{\rm QED}\,\text{MeV}\,, \tag{490}$$

$$f_\pi^{\rm isoQCD} = 130.56(2)_{\rm exp}(13)_{\rm QED}(2)_{V_{ud}}\,\text{MeV}\,, \tag{491}$$

$$f_K^{\rm isoQCD}\,|V_{us}| = \;\; 35.09(4)_{\rm exp}(4)_{\rm QED}\,\text{MeV}\,, \tag{492}$$

$$f_K^{\rm isoQCD} = 157.2(2)_{\rm exp}(2)_{\rm QED}(4)_{V_{us}}\,\text{MeV}\,, \tag{493}$$

where we have used the PDG values [15] for $f_x|V_y|$ (equivalent to Eqs. (486) and (487)), and the values

$$V_{ud} = 0.97370(14)\,, \quad V_{us} = 0.2232(6)\,.$$

Here, V_{ud} is from the PDG [15] (beta decays) and the latter from Sec. 4 ($f_+(0)$ for $N_f = 2+1+1$). Of course, the information on pion and kaon leptonic decays do not enter the determinations of V_{ud} and V_{us} used here. The uncertainties in the above values are in the following assumed to have been considered in the estimates of the scale given by the collaborations. This is analogous to the systematics due to excited-state contaminations in hadron masses, an issue which is irrelevant in the pseudoscalar channel (see Fig. 50).

Depending on the lattice formulation, there is also a nontrivial renormalization of the axial current. Since it is easily determined from a chiral Ward identity, it does not play an important rôle. When it is present, it is assumed to be accounted for in the statistical errors.

11.4.3 Other physics scales

Scales derived from bottomonium have been used in the past, in particular, the splitting $\Delta m_\Upsilon = m_{\Upsilon(2s)} - m_{\Upsilon(1s)}$. They have very little dependence on the light-quark masses, but need an input for the b-quark mass. In all relevant cases, the b quark is treated by NRQCD.

11.5 Theory scales

In the following, we consider in more detail the two classes of theory scales that are most commonly used in typical lattice computations. The first class consists of scales related to the static quark-antiquark potential [12]. The second class is related to the action density renormalized through the gradient flow [42].

11.5.1 Potential scales

In this approach, lattice scales are derived from the properties of the static quark-antiquark potential. In particular, a scale can be defined by fixing the force $F(r)$ between a static quark and antiquark separated by the distance r in physical units [12]. Advantages of using the potential include the ease and accuracy of its computation, and its mild dependence on the valence-quark mass. In general, a potential scale r_c can be fixed through the condition that the static force takes a predescribed value, i.e.,

$$r_c^2 F(r_c) = X_c \tag{494}$$

where X_c is a suitably chosen number. Phenomenological and computational considerations suggest that the optimal choice for X_c is in the region where the static force turns over from Coulomb-like to linear behaviour and before string breaking occurs. In the original work [12], it was suggested to use $X_0 = 1.65$ leading to the condition

$$r_0^2 F(r_0) = 1.65\,. \tag{495}$$

In Ref. [43], the value $X_1 = 1.0$ was proposed yielding the scale r_1.

The static force is the derivative of the static quark-antiquark potential $V(r)$ which can be determined through the calculation of Wilson loops. More specifically, the potential at distance r is extracted from the asymptotic time dependence of the $r \times t$-sized Wilson loops $W(r,t)$,

$$V(r) = -\lim_{t\to\infty} \frac{d}{dt} \log\langle W(r,t)\rangle\,. \tag{496}$$

The derivative of the potential needed for the force is then determined through the derivative of a suitable local parameterization of the potential as a function of r, e.g.,

$$V(r) = C_- \frac{1}{r} + C_0 + C_+ r\,, \tag{497}$$

estimating uncertainties due to the parameterization. In some calculations, the gauge field is fixed to Coulomb or temporal gauge in order to ease the computation of the potential at arbitrary distances.

In order to optimize the overlap of the Wilson loops with the ground state of the potential, one can use different types and levels of spatial gauge field smearing and extract the ground state energy from the corresponding correlation matrix by solving a generalized eigenvalue

problem [44–46]. Finally, one can also make use of the noise reduction proposed in Refs. [47, 48]. It changes the definition of the discretized loops by a smearing of the temporal parallel transporter [49] and thus yields a different discretization of the continuum force.

11.5.2 Gradient flow scales

The gradient flow $B_\mu(t,x)$ of gauge fields is defined in the continuum by the flow equation

$$\dot{B}_\mu = D_\nu G_{\nu\mu}, \quad B_\mu|_{t=0} = A_\mu\,, \tag{498}$$

$$G_{\mu\nu} = \partial_\mu B_\nu - \partial_\nu B_\mu + [B_\mu, B_\nu], \quad D_\mu = \partial_\mu + [B_\mu, \cdot\,]\,, \tag{499}$$

where A_μ is the fundamental gauge field, $G_{\mu\nu}$ the field strength tensor, and D_μ the covariant derivative [42]. At finite lattice spacing, a possible form of Eqs. (498) and (499) is

$$a^2 \frac{d}{dt} V_t(x,\mu) = -g_0^2 \cdot \partial_{x,\mu} S_G(V_t) \cdot V_t(x,\mu)\,, \tag{500}$$

where $V_t(x,\mu)$ is the flow of the original gauge field $U(x,\mu)$ at flow time t, S_G is an arbitrary lattice discretization of the gauge action, and $\partial_{x,\mu}$ denotes the su(3)-valued differential operator with respect to $V_t(x,\mu)$. An important point to note is that the flow time t has the dimension of a length squared, i.e., $t \sim a^2$, and hence provides a means for setting the scale.

One crucial property of the gradient flow is that any function of the gauge fields evaluated at flow times $t > 0$ is renormalized [50] by just renormalizing the gauge coupling. Therefore, one can define a scale by keeping a suitable gluonic observable defined at constant flow time t, e.g., the action density $E = -\frac{1}{2}\operatorname{Tr} G_{\mu\nu}G_{\mu\nu}$ [42], fixed in physical units. This can, for example, be achieved through the condition

$$t_c^2 \langle E(t_c,x)\rangle = c\,, \quad E(t,x) = -\frac{1}{2}\operatorname{Tr} G_{\mu\nu}(t,x) G_{\mu\nu}(t,x) \tag{501}$$

where $G_{\mu\nu}(t,x)$ is the field strength tensor evaluated on the flown gauge field V_t. Then, the lattice scale a can be determined from the dimensionless flow time in lattice units, $\hat{t}_c = a^2 t_c$. The original proposal in [42] was to use $c = 0.3$ yielding the scale t_0,

$$t_0^2 \langle E(t_0)\rangle = 0.3\,. \tag{502}$$

For convenience one sometimes also defines $s_0 = \sqrt{t_0}$.

An alternative scale w_0 has been introduced in Ref. [39]. It is defined by fixing a suitable derivative of the action density,

$$W(t_c) = t_c \cdot \partial_t \left(t^2 \langle E(t)\rangle\right)_{t=t_c} = c\,. \tag{503}$$

Setting $c = 0.3$ yields the scale w_0 through

$$W(w_0^2) = 0.3\,. \tag{504}$$

In addition to the lattice scales from t_0 and w_0, one can also consider the scale from the dimensionful combination t_0/w_0. This combination has been found to have a very weak dependence on the quark mass [51–53].

A useful property of the gradient flow scales is the fact that their quark-mass dependence is known from χPT [54].

Since the action density at $t \sim t_0 \sim w_0^2$ usually suffers from large autocorrelation [51, 55], the calculation of the statistical error needs special care.

Lattice artefacts in the gradient flow scales originate from different sources [56], which are systematically discussed by considering t as a coordinate in a fifth dimension. First, there is the choice of the action S_G for $t > 0$. Second, there is the discretization of $E(t, x)$. Third, there is the discretization of the 4-dimensional quantum action, which is always there, and fourth, there are also terms localized at the boundary $t = 0_+$. The interplay between the different sources of lattice artefacts turns out to be rather subtle [56].

Removing discretization errors due to the first two sources requires only classical (g_0-independent) improvement. Those due to the quantum action are common to all $t = 0$ observables, but the effects of the boundary terms are not easily removed in practice. At tree level, the Zeuthen flow [56] does the complete job, but none of the computations reviewed here have used it. Discretization effects due to S_G can be removed by using an improved action such as the tree-level Symanzik-improved gauge action [39, 57]. More phenomenological attempts of improving the gradient flow scales consist of applying a t-shift [58], or tree-level improvement [59].

11.5.3 Other theory scales

The MILC collaboration has been using another set of scales, the partially quenched pseudoscalar decay constant f_{p4s} with degenerate valence quarks with a mass $m_q = 0.4 \cdot m_{\text{strange}}$, and the corresponding partially quenched pseudoscalar mass M_{p4s}. So far it has been a quantity only used by the MILC collaboration [60–62]. We do not perform an in-depth discussion or an average but will list numbers in the results section.

Yet another scale that has been used is the leptonic decay constant of the η_s. This fictitious particle is a pseudoscalar made of a valence quark-antiquark pair with different (fictitious) flavours which are mass-degenerate with the strange quark [63–65].

11.6 List of computations and results

11.6.1 Gradient flow scales

We now turn to a review of the calculations of the gradient flow scales $\sqrt{t_0}$ and w_0. The results are compiled in Tab. 76 and shown in Fig. 51. In the following, we briefly discuss the calculations in the order that they appear in the table and figure.

ETM 21 [53] finalizes and supersedes ETM 20 discussed below. It determines the scales $\sqrt{t_0}, w_0$, also $t_0/w_0 = 0.11969(62)$ fm, and the ratio $\sqrt{t_0}/w_0 = 0.82930(65)$, cf. also HPQCD 13A [68]. Since ETM 21 is now published, the values replace the ones of ETM 20 in the FLAG averages given in this web update.

CalLat 20A [31] use Möbius Domain-Wall valence fermions on HISQ ensembles generated by the MILC and CalLat collaborations. The gauge fields entering the Möbius Domain-Wall operator are gradient-flow smeared with $t = a^2$. They compute the Ω mass and the scales w_0, t_0 and perform global fits to determine $w_0 M_\Omega$ and $\sqrt{t_0} M_\Omega$ at the physical point. The flow is discretized with the Symanzik tree-level improved action and the clover discretization of $E(t)$ is used. A global fit with Bayesian priors is performed including terms derived from χPT for finite volume and quark-mass dependences, as well as a^2 and $a^2\alpha_s(1.5/a)$ terms for discretization errors. Also, a tree-level improved definition of the GF scales is used where the leading-in-g^2 cutoff effects are removed up to and including $\mathcal{O}(a^8/t^4)$.

Collaboration	Ref.	N_f	publication status	chiral extrapolation	continuum extrapolation	finite volume	physical scale	$\sqrt{t_0}$ [fm]	w_0 [fm]
ETM 21	[53]	2+1+1	A	★	★	★	f_π	0.14436(61)	0.17383(63)
CalLat 20A	[31]	2+1+1	A	★	★	★	m_Ω	0.1422(14)	0.1709(11)
BMW 20	[3]	1+1+1+1	A	★	★	★	m_Ω		0.17236(29)(63)[70]
ETM 20	[1053]	2+1+1	C	★	★	★	f_π		0.1706(18)
MILC 15	[67]	2+1+1	A	★	★	★	$F_{p4s}(f_\pi)^\#$	0.1416(+8/-5)	0.1714(+15/-12)
HPQCD 13A	[68]	2+1+1	A	★	○	★	f_π	0.1420(8)	0.1715(9)
RQCD 22	[69]	2+1	P	★	★	★	m_Ξ	0.1449(+7/-9)	
CLS 21	[70]	2+1	C	★	★	★	f_π, f_K	0.1443(7)(13)	
CLS 16	[71]	2+1	A	○	★	★	f_π, f_K	0.1467(14)(7)	
QCDSF/UKQCD 15B	[72]	2+1	P	○	○	○	$m_P^{SU(3)}$	0.1511(22)(6)(5)(3)	0.1808(23)(5)(6)(4)
RBC/UKQCD 14B	[32]	2+1	A	★	★	★	m_Ω	0.14389(81)	0.17250(91)
HotQCD 14	[73]	2+1	A	★	★	★	$r_1(f_\pi)^\#$		0.1749(14)
BMW 12A	[39]	2+1	A	★	★	★	m_Ω	0.1465(21)(13)	0.1755(18)(4)

Table 76: Results for gradient flow scales at the physical point, cf. Eq. (469). Note that BMW 20 [3] take IB and QED corrections into account. Some additional results for ratios of scales are:
ETM 21 [53]: $t_0/w_0 = 0.11969(62)$ fm.
$^\#$ These scales are not physical scales and have been determined from f_π.

BMW 20 [3] presents a result for w_0 in the context of their staggered fermion calculation of the muon anomalous magnetic moment. It is the first computation that takes QED and isospin-breaking corrections into account. The simulations are performed by using staggered fermions with stout gauge field smearing with six lattice spacings and several pion masses around the physical point with M_π between 110 and 140 MeV. Volumes are around $L = 6$ fm. At the largest lattice spacing, it is demonstrated how the effective masses of the Ω correlator almost reach the plateau value extracted from a four-state fit (two states per parity). Within the range where the data is fitted, the deviation of data points from the estimated plateau is less than a percent. Isospin-breaking corrections are computed by Taylor expansion around isoQCD with QED treated as $\mathrm{QED_L}$. Finite volume effects in QED are taken from the $1/L, 1/L^2$ universal corrections and $\mathcal{O}(1/L^3)$ effects are neglected. The results for $M_\Omega w_0$ are extrapolated to the continuum by a fit with a^2 and a^4 terms.

ETM 20 [1053] presents in their proceedings contribution a preliminary analysis of their $N_f = 2 + 1 + 1$ Wilson twisted-mass fermion simulations at maximal twist (i.e., automatic $\mathcal{O}(a)$ improved), at three lattice spacings and pion masses at the physical point. Their determination of $w_0 = 0.1706(18)$ fm from f_π using an analysis in terms of M_π is the value quoted above. They obtain the consistent value $w_0 = 0.1703(18)$ fm from an analysis in terms of the renormalized light quark mass.

MILC 15 [67] sets the physical scale using the fictitious pseudoscalar decay constant $F_{p4s=}153.90(9)(+21/-28)$ MeV with degenerate valence quarks of mass $m_v = 0.4m_s$ and physical sea-quark masses [62]. (F_{p4s} has strong dependence on the valence-quark mass and

is determined from f_π.) They use a definition of the flow scales where the tree-level lattice artefacts up to $\mathcal{O}(a^4/t^2)$ are divided out. Charm-quark mass mistunings are between 1% and 11%. They are taken into account at leading order in $1/m_c$ through $\Lambda^{(3)}_{\rm QCD}$ applied directly to F_{p4s} and $1/m_c$ corrections are included as terms in the fits. They use elaborate variations of fits in order to estimate extrapolation errors (both in GF scales and F_{p4s}). They include errors from FV effects and experimental errors in f_π in F_{p4s}.

HPQCD 13A [68] uses eight MILC-HISQ ensembles with lattice spacings $a = 0.088$, 0.121, 0.151 fm. Values of L are between 2.5 fm and 5.8 fm with $M_\pi L = 3.3$–4.6. Pion masses range between 128 and 306 MeV. QCD is defined by using the inputs $M_\pi = 134.98(32)$ MeV, $M_K = 494.6(3)$ MeV, $f_{\pi^+} = 130.4(2)$ MeV derived by model subtractions of IB effects. Additional scale ratios are given: $\sqrt{t_0}/w_0 = 0.835(8)$, $r_1/w_0 = 1.789(26)$.

RQCD 22 [69] is an independent analysis of CLS ensembles employing $N_f = 2+1$ non-perturbatively improved Wilson fermions and the tree-level Symanzik improved gauge action. It uses a multitude of quark-mass combinations at six different values of the lattice spacing, ranging from $a \lesssim 0.098$ fm down to $a < 0.039$ fm. Near-physical quark masses are realized at $a = 0.064$ fm and $a = 0.085$ fm. The input quantities used to fix the physical point and to set the scale are $M_\pi = 134.8(3)$ MeV, $M_K = 494.2(3)$ MeV, and $m_\Xi = 1316.9(3)$ MeV (last line of pg. 33 in [69]). Since RQCD 22 is not yet published at the time of this web update, the result for $\sqrt{t_0}$ is not included in the FLAG average.

CLS 21 [70] is a proceedings contribution describing a preliminary analysis following the one in CLS 16 [71], cf. the description below. CLS 21 includes about double the amount of ensembles as compared to CLS 16, in particular ensembles at two more lattice spacings and two ensembles at the physical point. As a consequence, this analysis is not considered a straightforward update and hence does not supersede the result of CLS 16.

CLS 16 [71] uses CLS configurations of 2+1 nonperturbatively $\mathcal{O}(a)$-improved Wilson fermions. There are a few pion masses with the strange mass adjusted along a line of $m_u + m_d + m_s = \text{const}$. Three different lattice spacings are used. They determine t_0 at the physical point defined by π and K masses and the linear combination $f_K + \frac{1}{2} f_\pi$. They use the Wilson flow with the clover definition of $E(t)$.

QCDSF 15B [72, 74] results, unpublished, are obtained by simulating $N_f = 2+1$ QCD with the tree-level Symanzik improved gauge action and clover Wilson fermions with single level stout smearing for the hopping terms together with unsmeared links for the clover term (SLiNC action). Simulations are performed at four different lattice spacings, in the range $[0.06, 0.08]$ fm, with $M_{\pi,\rm min} = 228$ MeV and $M_{\pi,\rm min} L = 4.1$. The results for the gradient flow scales have been obtained by relying on the observation that flavour-symmetric quantities get corrections of $\mathcal{O}((\Delta m_q)^2)$ where Δm_q is the difference of the quark mass from the $SU(3)$-symmetric value. The $\mathcal{O}(\Delta m_q^2)$ terms are not detected in the data and subsequently neglected.

RBC/UKQCD 14B [32] presents results for $\sqrt{t_0}$ and w_0 obtained in QCD with $2+1$ dynamical flavours. The simulations are performed by using domain-wall fermions on six ensembles with lattice spacing $a^{-1} = 1.38, 1.73, 1.78, 2.36, 2.38$, and 3.15 GeV, pion masses in the range $M_\pi^{unitary} \in [139, 360]$ MeV. The simulated volumes are such that $M_\pi L > 3.9$. The effective masses of the Ω correlator are extracted with two-state fits and it is shown, by using two different nonlocal interpolating operators at the source, that the correlators almost reach a pleateau. In the calculation of $\sqrt{t_0}$ and w_0, the clover definition of $E(t)$ is used. The values given are $\sqrt{t_0} = 0.7292(41)\,\text{GeV}^{-1}$ and $w_0 = 0.8742(46)\,\text{GeV}^{-1}$ which we converted to the values in Tab. 76.

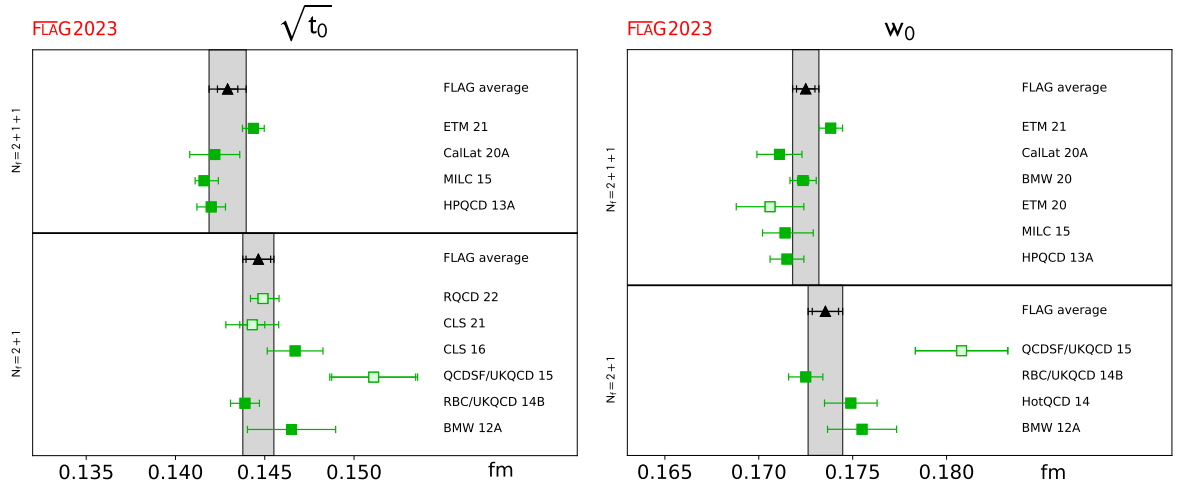

Figure 51: Results for gradient flow scales.

HotQCD 14 [73] determines the equation of state with $N_f = 2+1$ flavours using highly improved staggered quarks (HISQ/tree). As a byproduct, they update the results of HotQCD 11 [75] by adding simulations at four new values of β, for a total of 24 ensembles, with lattice spacings in the range $[0.04, 0.25]$ fm and volumes in the range $[2.6, 6.1]$ fm with $M_\pi = 160$ MeV. They obtain values for the scale parameters r_0 and w_0, via the ratios $r_0/r_1, w_0/r_1$ and using $r_1 = 0.3106(14)(8)(4)$ fm from MILC 10 [76]. They obtain for the ratios $(r_0/r_1)_{cont} = 1.5092(39)$ and $(w_0/r_1)_{cont} = 0.5619(21)$ in the continuum. They cross-check their determination of the scale r_1 using the hadronic quantities f_K, f_η from HPQCD 09B [64] and the experimental value of M_φ, and find good agreement.

BMW 12A [39] is the work in which w_0 was introduced. Simulations with 2HEX smeared Wilson fermions and two-level stout-smeared rooted staggered fermions are done. The Wilson flow with clover $E(t)$ is used, and a test of the Symanzik flow is carried out. They take the results with Wilson fermions as their central value, because those "do not rely on the 'rooting' of the fermion determinant". Staggered fermion results agree within uncertainties.

11.6.2 Potential scales

We now turn to a review of the calculations of the potential scales r_0 and r_1. The results are compiled in Tab. 77 and shown in Fig. 52. The most recent calculations date back to 2014, and we discuss them in the order that they appear in the table and the figure.

ETM 14 [34] uses $N_f = 2+1+1$ Wilson twisted-mass fermions at maximal twist (i.e., automatic $\mathcal{O}(a)$-improved), three lattice spacings and pion masses reaching down to $M_\pi = 211$ MeV. They determine the scale r_0 through $f_\pi = f_{\pi^+} = 130.41$ MeV. A crosscheck of the so obtained lattice spacings with the ones obtained via the fictitious pseudoscalar meson $M_{s's'}$ made of two strange-like quarks gives consistent results. The crosscheck is done using the dimensionless combinations $r_0 M_{s's'}$ (with r_0 in the chiral limit) and $f_\pi/M_{s's'}$ determined in the continuum, and then using r_0/a and the value of $M_{s's'}$ obtained from the experimental value of f_π. We also note that in Ref. [51] using the same ensembles the preliminary value $w_0 = 0.1782$ fm is determined, however, without error due to the missing or incomplete investigation of the systematic effects.

Collaboration	Ref.	N_f	publication status	chiral extrapolation	continuum extrapolation	finite volume	physical scale	r_0 [fm]	r_1 [fm]
ETM 14	[34]	2+1+1	A	○	★	★	f_π	0.474(14)	
HPQCD 13A	[68]	2+1+1	A	★	○	★	f_π		0.3112(30)
HPQCD 11B	[63]	2+1+1	A	○	○	○	ΔM_Υ, f_{η_s}		0.3209(26)
HotQCD 14	[73]	2+1	A	★	★	★	r_1([76])$^\#$	0.4688(41)	
χQCD 14	[77]	2+1	A	○	○	○	three inputs[5]	0.465(4)(9)	
HotQCD 11	[75]	2+1	A	★	★	★	f_π	0.468(4)	
RBC/UKQCD 10A	[40]	2+1	A	○	○	○	M_Ω	0.487(9)	0.333(9)
MILC 10	[76]	2+1	C	○	★	★	f_π		0.3106(8)(14)(4)
MILC 09	[78]	2+1	A	○	★	★	f_π		$0.3108(15)(^{+26}_{-79})$
MILC 09A	[35]	2+1	C	○	★	★	f_π		$0.3117(6)(^{+12}_{-31})$
HPQCD 09B	[64]	2+1	A	○	★	○	three inputs		0.3133(23)(3)
PACS-CS 08	[33]	2+1	A	★	■	■	M_Ω	$0.4921(64)(^{+74}_{-2})$	
HPQCD 05B	[65]	2+1	A	○	○	○	ΔM_Υ	0.469(7)	0.321(5)
Aubin 04	[79]	2+1	A	○	○	○	ΔM_Υ	0.462(11)(4)	0.317(7)(3)

Table 77: Results for potential scales at the physical point, cf. Eq. (469). $\Delta M_\Upsilon = M_{\Upsilon(2s)} - M_{\Upsilon(1s)}$.
$^\#$ This theory scale was determined in turn from r_1 [76].

HPQCD 13A [68] was already discussed above in connection with the gradient flow scales.

HPQCD 11B [63] uses five MILC-HISQ ensembles and determines r_1 from $M_{\Upsilon(2s)} - M_{\Upsilon(1s)}$ and the decay constant f_{η_s} (see HPQCD 09B). The valence b quark is treated by NRQCD, while the light valence quarks have the HISQ discretization, identical to the sea quarks.

HotQCD 14 [73] was already discussed in connection with the gradient flow scales.

χQCD 14 [77] uses overlap fermions as valence quarks on $N_f = 2+1$ domain-wall fermion gauge configurations generated by the RBC/UKQCD collaboration [40]. Using the physical masses of D_s, D_s^* and J/ψ as inputs, the strange and charm quark masses and the decay contant f_{D_s} are determined as well as the scale r_0.

HotQCD 11 [75] uses configurations with tree-level improved Symanzik gauge action and HISQ staggered quarks in addition to previously generated ensembles with p4 and asqtad staggered quarks. In this calculation, QCD is defined by generating lines of constant physics with $m_l/m_s = \{0.2, 0.1, 0.05, 0.025\}$ and setting the strange quark mass by requiring that the mass of a fictious $\eta_{s\bar{s}}$ meson is $M_{\eta_{s\bar{s}}} = \sqrt{2M_K^2 - M_\pi^2}$. The physical point is taken to be at $m_l/m_s = 0.037$. The physical scale is set by using the value $r_1 = 0.3106(8)(18)(4)$ fm obtained in Ref. [76] by using f_π as physical input. In the paper, this result is shown to be consistent within the statistical and systematic errors with the choice of f_K as physical input. The result $r_0/r_1 = 1.508(5)$ is obtained by averaging over 12 ensembles at $m_l/m_s = 0.05$ with lattice spacings in the range $[0.066, 0.14]$ fm. This result is then used to get $r_0 = 0.468(4)$ fm. Finite volume effects have been monitored with 20 ensembles in the range $[3.2, 6.1]$fm with $M_\pi L > 2.6$.

RBC/UKQCD 10A [40] uses $N_f = 2+1$ flavours of domain-wall quarks and the Iwasaki

gauge action at two values of the lattice spacing with unitary pion masses in the approximate range $[290, 420]$ MeV. They use the masses of π and K meson and of the Ω baryon to determine the physical quark masses and the lattice spacings, and so obtain estimates of the scales r_0, r_1 and the ratio r_1/r_0 from a combined chiral and continuum extrapolation.

MILC 10 [76] presents a further update of r_1 with asqtad staggered quark ensembles with $a \in \{0.045, 0.06, 0.09\}$ fm. It supersedes MILC 09 [35, 78, 80].

MILC 09 [78] presents an $N_f = 2+1$ calculation of the potential scales on asqtad staggered quark ensembles with $a \in \{0.045, 0.06, 0.09, 0.12, 0.15, 0.18\}$ fm. The continuum extrapolation is performed by using Goldstone boson pions as light as $M_\pi = 224$ MeV (RMS pion mass of 258 MeV). The physical scale is set from f_π. The result for r_1 obtained in the published paper [78] is then updated and, therefore, superseded by the conference proceedings MILC 09A and 09B [35, 80].

HPQCD 09B [64] is an extension of HPQCD 05B [65] and uses HISQ valence quarks instead of asqtad quarks. The scale r_1 is obtained from three different inputs. First $r_1 = 0.309(4)$ fm from the splitting of 2S and 1S Υ states as in Ref. [65], second $r_1 = 0.316(5)$ fm from $M_{D_s} - M_{\eta_s}/2$ and third $r_1 = 0.315(3)$ fm from the decay constant of the η_s. The ficitious η_s state is operationally defined by setting quark masses to the s-quark mass and dropping disconnected diagrams. Its mass and decay constant are obtained from a partially quenched chiral perturbation theory analysis using the pion and kaon states from experiment together with various partially quenched lattice data. The three results are combined to $r_1 = 0.3133(23)(3)$ fm.

PACS-CS 08 [33] presents a calculation of r_0 in $N_f = 2 + 1$ QCD by using NP $\mathcal{O}(a)$-improved clover Wilson quarks and Iwasaki gauge action. The calculation is done at fixed lattice spacing $a = 0.09$ fm and is extrapolated to the physical point from (unitary) pion masses in the range $[156, 702]$ MeV. The $N_f = 2+1$ theory is defined by fixing M_π, M_K, and M_Ω to 135.0, 497.6, and 1672.25 MeV, respectively. The effective masses of smeared-local Ω correlators averaged over the four spin polarizations show quite good plateaux.

HPQCD 05B [65] performed the first bottomonium spectrum calculation in full QCD with $N_f = 2 + 1$ on MILC asqtad configurations and the b quark treated by NRQCD. They find agreement of the low lying Υ states with experiment and also compare to quenched and $N_f = 2$ results. They determined r_0 and r_1 from the splitting of 2S and 1S states.

Aubin 04 [79] presents an $N_f = 2 + 1$ calculation of the potential scales by using asqtad staggered quark ensembles with $a = 0.09$ and $0.12\}$ fm. The continuum extrapolation is performed by using Goldstone boson pions as light as $m_\pi = 250$ MeV. The physical scale is set from the Υ 2S-1S and 1P-1S splittings computed with NRQCD by HPQCD [81].

11.6.3 Ratios of scales

It is convenient in many cases to also have ratios of scales at hand. In addition to translating from one scale to another, the ratios provide important crosschecks between different determinations. Results on ratios provided by the collaborations are compiled in Tab. 78 and Fig. 53. The details of the computations were already discussed in the previous sections.

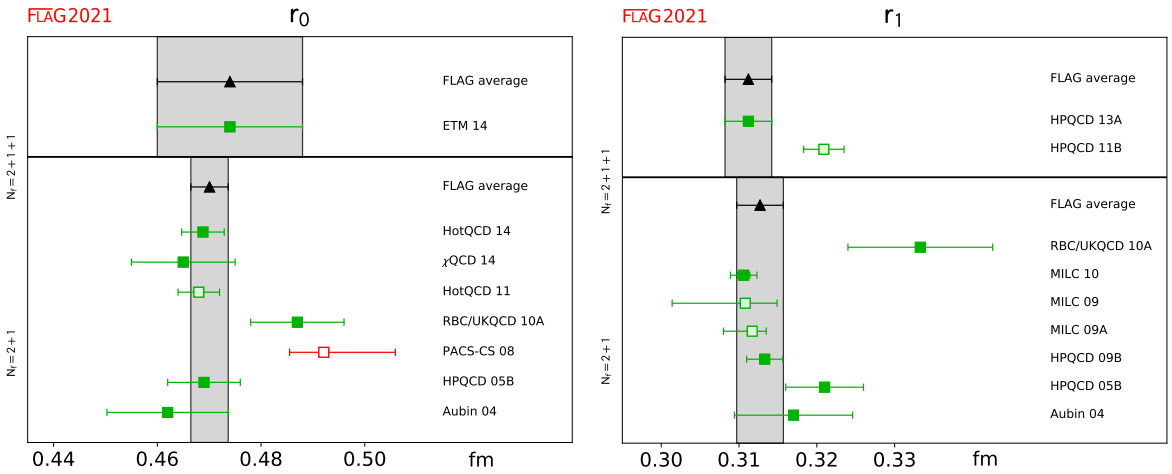

Figure 52: Results for potential scales.

Collaboration	Ref.	N_f	publication status	chiral extrapolation	continuum extrapolation	finite volume	$\sqrt{t_0}/w_0$	r_0/r_1	r_1/w_0
ETM 21	[53]	2+1+1	A	★	★	★	0.82930(65)		
HPQCD 13A	[68]	2+1+1	A	★	○	★	0.835(8)		1.789(26)
HotQCD 14	[73]	2+1	A	★	★	★			1.7797(67)
HotQCD 11	[75]	2+1	A	★	★	★		1.508(5)	
RBC/UKQCD 10A	[40]	2+1	A	○	○	○		1.462(32)$^{\#}$	
Aubin 04	[79]	2+1	A	○	○	○		1.474(7)(18)	

Table 78: Results for dimensionless ratios of scales.
$^{\#}$This value is obtained from $r_1/r_0 = 0.684(15)(0)(0)$.

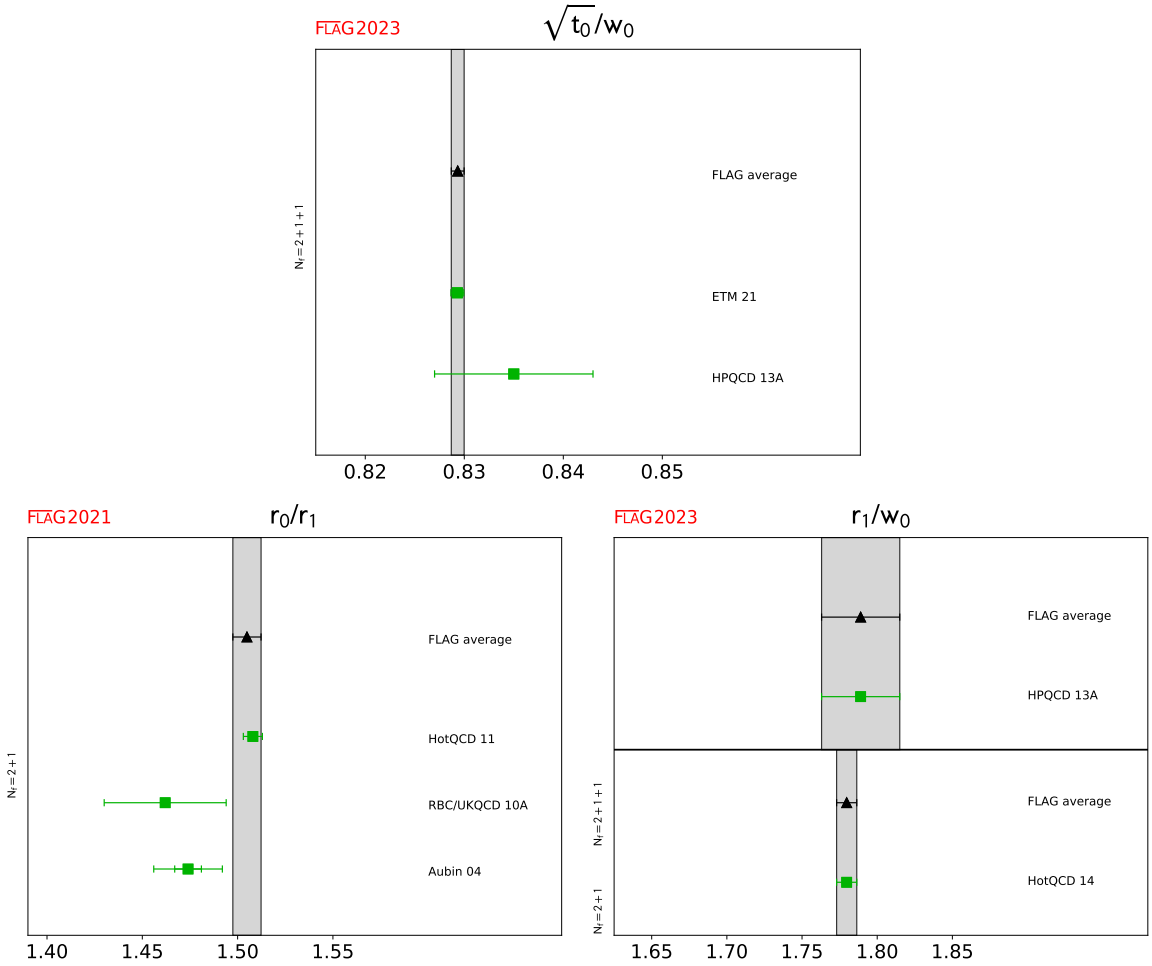

Figure 53: Results for dimensionless ratios of scales.

11.7 Averages

Gradient flow scale $\sqrt{t_0}$

For $N_f = 2+1+1$, we have two recent calculations from ETM 21 [53] and CalLat 20A [31], and two less recent ones from MILC 15 [67] and HPQCD 13A [68] fulfilling the FLAG criteria to enter the average. The latter two and CalLat 20A are based on the same MILC-HISQ gauge field ensembles, hence we consider their statistical errors to be 100% correlated.

For $N_f = 2+1$, we have three calculations from CLS 16 [71], RBC/UKQCD 14B [32], and BMW 12A [39] which enter the FLAG average. All three are independent computations, so there is no correlation to be taken into account. QCDSF/UKQCD 15B [72] does not contribute to the average, because it is not published. CLS 21 [70] is a proceedings contribution based on double the number of ensembles. It is therefore not a straightforward update and does not supersede CLS 16 [71]. The new result by RQCD 22 [69] was not published by the date of this web update, January 2023, and is also not yet included in the average.

Performing the weighted and correlated average we obtain

$$N_f = 2+1+1: \qquad \sqrt{t_0} = 0.14292(104)\ \text{fm} \qquad \text{Refs. [31, 53, 67, 68]}, \tag{505}$$

$$N_f = 2+1: \qquad \sqrt{t_0} = 0.14464(87)\ \text{fm} \qquad \text{Refs. [32, 39, 71]}. \tag{506}$$

We note that the $N_f = 2+1+1$ results of staggered fermions and the twisted-mass result are not well compatible. The resulting stretching factor based on the χ^2 value from the weighted average for $N_f = 2+1+1$ is 1.81. It causes the error of this web update to be increased compared to FLAG 21. For the $N_f = 2+1$ average the stretching factor is 1.25. We hope that the differences for $N_f = 2+1+1$ get resolved in the near future and the uncertainty of the average decreases.

Gradient flow scale w_0

For $N_f = 1+1+1+1$, including QED, there is a single calculation, BMW 20 [3] with the result

$$N_f = 1+1+1+1+\text{QED}: \qquad w_0 = 0.17236(70)\ \text{fm} \qquad \text{Ref. [3]}. \tag{507}$$

For $N_f = 2+1+1$ we now have four calculations ETM 21 [53], CalLat 20A [31], MILC 15 [67], and HPQCD 13A [68] entering the FLAG average. The proceedings ETM 20 is superseded by ETM 21. As discussed above in connection with $\sqrt{t_0}$ we correlate the statistical errors of CalLat 20A, MILC 15, and HPQCD 13A.

For $N_f = 2+1$, we have three calculations RBC/UKQCD 14B [32], HotQCD 14 [73], and BMW 12A [39] that enter the FLAG average. These calculations are independent, and no correlation needs to be taken into account. QCDSF/UKQCD 15B [72] does not contribute to the average, because it is not published.

Performing the weighted and correlated average, we obtain

$$N_f = 2+1+1: \qquad w_0 = 0.17256(103)\ \text{fm} \qquad \text{Refs. [31, 53, 67, 68]}, \tag{508}$$

$$N_f = 2+1: \qquad w_0 = 0.17355(92)\ \text{fm} \qquad \text{Refs. [32, 39, 73]}. \tag{509}$$

As above $N_f = 2+1+1$ results of staggered fermions and the twisted-mass result are not well compatible. The resulting stretching factor based on the χ^2 value from the weighted average is 1.67. It causes the error of this web update to be slightly increased compared to FLAG

21. For the $N_f = 2+1$ average the stretching factor is 1.23. We hope that the differences for $N_f = 2+1+1$ get resolved in the near future and the uncertainty of the average decreases.

Isospin-breaking and electromagnetic corrections are expected to be small at the level of present uncertainties. This is also confirmed by the explicit computation by BMW 12A. Therefore, we also perform an average over all $N_f > 2+1$ computations and obtain

$$N_f > 2+1: \qquad w_0 = 0.17250(70)\ \text{fm} \qquad \text{Refs. [3, 31, 53, 67, 68].} \tag{510}$$

For the $N_f > 2+1$ average the rescaling factor is 1.45.

Gradient flow scale t_0/w_0

Currently, there is only one calculation of the scale t_0/w_0 available from ETM 21 [53] which forms the FLAG average

$$N_f = 2+1+1: \qquad t_0/w_0 = 0.11969(62)\ \text{fm} \qquad \text{Ref. [53].} \tag{511}$$

Potential scale r_0

For $N_f = 2+1+1$, there is currently only one determination of r_0 from ETM 14 [34], namely $r_0 = 0.474(14)$ fm, which, therefore, represents the FLAG average.

For $N_f = 2+1$, all but one calculation fulfill all the criteria to enter the FLAG average. HotQCD 14 [73] is essentially an update of HotQCD 11 [75] by enlarging the set of ensembles used in the computation. Therefore, the result from HotQCD 14 supersedes the one from HotQCD 11 and, hence, we only use the former in the average. The computation of χQCD [77] is based on the configurations produced by RBC/UKQCD 10A [40], and we, therefore, assume a 100% correlation between the statistical errors of the two calculations. HPQCD 05B [65] enhances the calculation of Aubin 04 [79] by adding ensembles at a coarser lattice spacing and using the same discretization for the valence fermion. Therefore, we consider the full errors (statistical and systematic) on the results from Aubin 04 and HPQCD 05B to be 100% correlated.

Performing the weighted and correlated average, we obtain

$$N_f = 2+1+1: \qquad r_0 = 0.474(14)\ \text{fm} \qquad \text{Ref. [34],} \tag{512}$$

$$N_f = 2+1: \qquad r_0 = 0.4701(36)\ \text{fm} \qquad \text{Refs. [40, 65, 73, 77, 79].} \tag{513}$$

We note that for the $N_f = 2+1$ average, the stretching factor based on the χ^2-value from the weighted average is 1.14.

Potential scale r_1

For $N_f = 2+1+1$, there are two works that fulfill the criteria to enter the FLAG average, namely HPQCD 13A [68] and HPQCD 11B [63]. Both are based on MILC-HISQ ensembles, the former uses eight, the latter only five. The result from HPQCD 13A supersedes the result from HPQCD 11B (in line with a corresponding statement in HPQCD 13A) and forms the FLAG average.

For $N_f = 2+1$, all the results quoted in Tab. 77 fulfill the FLAG criteria, but not all of them enter the average. The published result from MILC 09 [78] is superseded by the result in the proceedings MILC 10 [76], while MILC 09A [35] is a proceedings contribution and does not enter the average. HPQCD 09B [64] uses HISQ valence quarks instead of asqtad valence quarks as in HPQCD 05B [65]. Therefore, we have RBC/UKQCD 10A [40], MILC

10, HPQCD 09B, HPQCD 05B, and Aubin 04 entering the average. However, since the latter four calculations are based on the aqtad MILC ensembles, we attribute 100% correlation on the statistical error between them and 100% correlation on the systematic error between HPQCD 05B and Aubin 04 as discussed above in connection with r_0.

Performing the weighted and correlated average, we obtain

$$N_f = 2+1+1: \qquad r_1 = 0.3112(30)\ \text{fm} \qquad \text{Ref. [68]}, \tag{514}$$
$$N_f = 2+1: \qquad r_1 = 0.3127(30)\ \text{fm} \qquad \text{Refs. [40, 64, 65, 76, 79]}. \tag{515}$$

We note that for the $N_f = 2+1$ average the stretching factor based on the χ^2-value from the weighted average is 1.57.

The scales M_{p4s} and f_{p4s}

As mentioned in Sec. 11.5.3, these scales have been used only by the MILC and FNAL/MILC collaborations [60–62]. The latest numbers from Ref. [61] are $f_{4ps} = 153.98(11)(^{+2}_{-12})(12)[4]$ MeV and $M_{p4s} = 433.12(14)(^{+17}_{-6})(4)[40]$ MeV and, hence, we have

$$N_f = 2+1+1: \qquad f_{4ps} = 153.98(20)\ \text{MeV} \qquad \text{Ref. [61]}, \tag{516}$$
$$N_f = 2+1+1: \qquad M_{4ps} = 433.12(30)\ \text{MeV} \qquad \text{Ref. [61]}. \tag{517}$$

Dimensionless ratios of scales

We start with the ratio $\sqrt{t_0}/w_0$ for which two $N_f = 2+1+1$ calculations from ETM 21 [53] and HPQCD 13A [68] are available and form the FLAG average

$$N_f = 2+1+1: \qquad \sqrt{t_0}/w_0 = 0.82934(65) \qquad \text{Refs. [53, 68]}. \tag{518}$$

We note that here the error is reduced compared to FLAG 21 by an order of magnitude due to the very small error of ETM 21. It is further worth noting that the ETM 21 continuum extrapolated value is many standard deviations away from the results at finite lattice spacings, see Figs. 11-12 in Ref. [53].

For the ratio r_0/r_1 there are three calculations from HotQCD 11 [75], RBC/UKQCD 10A [40], and Aubin 04 [79] available. They all fulfill the FLAG criteria and enter the FLAG average of this ratio,

$$N_f = 2+1: \qquad r_0/r_1 = 1.5049(74) \qquad \text{Refs. [40, 75, 79]}. \tag{519}$$

We note that the stretching factor based on the χ^2-value from the weighted average is 1.54.

Finally, for the ratio r_1/w_0 there is one computation from HotQCD 14 [73] for $N_f = 2+1+1$, and one from HPQCD 13A [68] for $N_f = 2+1$ fulfilling the FLAG criteria, and, hence, forming the FLAG values

$$N_f = 2+1+1: \qquad r_1/w_0 = 1.789(26) \qquad \text{Ref. [68]}, \tag{520}$$
$$N_f = 2+1: \qquad r_1/w_0 = 1.7797(67) \qquad \text{Ref. [73]}. \tag{521}$$

11.8 Observations and conclusions

Unfortunately the different computations for theory scales reported here are generally not in good agreement within each set of 2+1+1 and 2+1 flavour content. As a measure we list here

the stretching factors above one. We remind the reader that their squares are equal to the χ^2/dof of the weighted averages. Quantitatively, the stretching factors are for $N_f = 2+1$: 1.3 (for $\sqrt{t_0}$), 1.2 (w_0), 1.1 (r_0), 1.6 (r_1), 1.5 (r_0/r_1). For $N_f = 2+1+1$ the numbers are larger: 1.8 ($\sqrt{t_0}$), 1.7 (w_0) and due to differences which exist between present days twisted-mass QCD results and staggered results. Of course, the limited number of large-scale QCD simulations that are available means that there are only a small number of truly independent determinations of the scales. For example, three out of the five computations entering our average for w_0 are based on the same HISQ rooted staggered fermion configurations and thus their differences are only due to the choice of the physical scale (m_Ω vs. f_π), the valence quark action (Möbius domain-wall valence fermions vs. staggered fermions) employed to compute it and different analysis of continuum limit, etc.

Due to the publication of ETM 21, differences between $N_f = 2+1$ and 2+1+1 QCD are now smaller and (within their errors) in agreement with expectations [82, 83]. The effect of the charm quark is $-0.6(8)\%$ on w_0 and $-1.2(9)\%$ on $\sqrt{t_0}$ as computed from the FLAG averages. Precision studies of the decoupling of charm quarks predicted generic effects of a magnitude of only $\approx 0.2\%$ [82, 83] for low energy quantities. Since the FLAG numbers have changed quite a bit due to one more computation entering the averages, we are looking forward to further and more precise results to see whether the numbers hold up over time. In this respect, it is highly desirable for future computations to also publish ratios such as $\sqrt{t_0}/w_0$ where numbers are rare so far.

Such ratios of gradient flow scales are also of high interest in order to better understand the specific discretization errors of gradient flow observables. So far, systematic studies and information on the different contributions (see Sec. 11.5.2 and Ref. [56]) are missing. A worrying result is, for example, the scale-setting study of Ref. [84] on ratios of scales. The authors find indications that the asymptotic $\sim a^2$ scaling does not set in before $a \approx 0.05$ fm and the $a = 0.04$ fm data has a relevant influence on their continuum extrapolations.

A final word concerns the physics scales that all results depend on. While the mass of the Ω baryon is more popular than the leptonic decay rate of the pion, both have systematics which are difficult to estimate. For the Ω baryon it is the contaminations by excited states and for the decay rates it is the QED effects $\delta f_\pi^{\rm isoQCD}$. The uncertainty in V_{ud} is *not* relevant at this stage, but means that one is relying more on the standard model being an accurate low energy theory than in the case of the Ω mass. In principle, excited state effects are controlled by just going to large Euclidean time, but, in practice, this yields errors that are too large. One, therefore, performs fits with a very small number of excitations while theoretically there is a multitude of multi-hadron states that are expected to contribute. For the leptonic decay rate of the pion, the situation is quite reversed, namely, the problematic QED contributions have a well-motivated theory: chiral perturbation theory. The needed combination of low-energy constants is not accessible from experiment but its large-N estimate [36] has been (indirectly) confirmed by the recent computation of $\delta f_\pi^{\rm isoQCD}$ [13]. Unfortunately the same comparison is not so favourable for the leptonic Kaon decay.

References

[1] T. Aoyama et al., *The anomalous magnetic moment of the muon in the Standard Model*, *Phys. Rept.* **887** (2020) 1 [2006.04822].

[2] M. Della Morte, A. Francis, V. Gülpers, G. Herdoíza, G. von Hippel, H. Horch et al., *The hadronic vacuum polarization contribution to the muon $g-2$ from lattice QCD*, *JHEP* **10** (2017) 020 [1705.01775].

[3] [BMW 20] Sz. Borsanyi et al., *Leading hadronic contribution to the muon magnetic moment from lattice QCD*, *Nature* **593** (2021) 51 [2002.12347].

[4] G.P. Lepage, *The Analysis of Algorithms for Lattice Field Theory*, in *Boulder ASI 1989:97-120*, pp. 97–120, 1989, http://alice.cern.ch/format/showfull?sysnb=0117836.

[5] M. Luscher, *Computational Strategies in Lattice QCD*, in *Les Houches Summer School: Session 93: Modern perspectives in lattice QCD: Quantum field theory and high performance computing*, 2, 2010 [1002.4232].

[6] B. Jäger, T.D. Rae, S. Capitani, M. Della Morte, D. Djukanovic, G. von Hippel et al., *A high-statistics study of the nucleon EM form factors, axial charge and quark momentum fraction*, *PoS* **LATTICE2013** (2014) 272 [1311.5804].

[7] S. Capitani, M. Della Morte, G. von Hippel, B. Knippschild and H. Wittig, *Scale setting via the Ω baryon mass*, *PoS* **LATTICE2011** (2011) 145 [1110.6365].

[8] [ALPHA 12] P. Fritzsch, F. Knechtli, B. Leder, M. Marinkovic, S. Schaefer et al., *The strange quark mass and the Λ parameter of two flavor QCD*, *Nucl.Phys.* **B865** (2012) 397 [1205.5380].

[9] [ALPHA 13A] S. Lottini, *Chiral behaviour of the pion decay constant in $N_f = 2$ QCD*, *PoS* **LATTICE2013** (2013) 315 [1311.3081].

[10] R. Sommer, *Scale setting in lattice QCD*, *PoS* **LATTICE2013** (2014) 015 [1401.3270].

[11] M. Creutz, *Monte Carlo Study of Quantized SU(2) Gauge theory*, *Phys. Rev.* **D21** (1980) 2308.

[12] R. Sommer, *A new way to set the energy scale in lattice gauge theories and its applications to the static force and α_s in SU(2) Yang-Mills theory*, *Nucl. Phys.* **B411** (1994) 839 [hep-lat/9310022].

[13] M. Di Carlo, D. Giusti, V. Lubicz, G. Martinelli, C. Sachrajda, F. Sanfilippo et al., *Light-meson leptonic decay rates in lattice QCD+QED*, *Phys. Rev. D* **100** (2019) 034514 [1904.08731].

[14] R.F. Dashen, *Chiral SU(3)×SU(3) as a symmetry of the strong interactions*, *Phys. Rev.* **183** (1969) 1245.

[15] Particle Data Group collaboration, *Review of Particle Physics*, *PTEP* **2020** (2020) 083C01.

[16] [BMW 14] Sz. Borsanyi et al., *Ab initio calculation of the neutron-proton mass difference*, *Science* **347** (2015) 1452 [1406.4088].

[17] Z. Davoudi and M.J. Savage, *Finite-Volume Electromagnetic Corrections to the Masses of Mesons, Baryons and Nuclei*, *Phys. Rev.* **D90** (2014) 054503 [1402.6741].

[18] B. Lucini, A. Patella, A. Ramos and N. Tantalo, *Charged hadrons in local finite-volume QED+QCD with C^* boundary conditions*, *JHEP* **02** (2016) 076 [1509.01636].

[19] M. Hayakawa and S. Uno, *QED in finite volume and finite size scaling effect on electromagnetic properties of hadrons*, *Prog. Theor. Phys.* **120** (2008) 413 [0804.2044].

[20] T. Blum et al., *Electromagnetic mass splittings of the low lying hadrons and quark masses from 2+1 flavor lattice QCD+QED*, *Phys. Rev.* **D82** (2010) 094508 [1006.1311].

[21] Z. Fodor, C. Hoelbling, S.D. Katz, L. Lellouch, A. Portelli, K.K. Szabo et al., *Quantum electrodynamics in finite volume and nonrelativistic effective field theories*, *Phys. Lett.* **B755** (2016) 245 [1502.06921].

[22] U.J. Wiese, *C periodic and G periodic QCD at finite temperature*, *Nucl. Phys. B* **375** (1992) 45.

[23] L. Polley, *Boundaries for SU(3)(C) x U(1)-el lattice gauge theory with a chemical potential*, *Z. Phys. C* **59** (1993) 105.

[24] M. Göckeler, R. Horsley, E. Laermann, P.E.L. Rakow, G. Schierholz, R. Sommer et al., *QED: A Lattice Investigation of the Chiral Phase Transition and the Nature of the Continuum Limit*, *Nucl. Phys.* **B334** (1990) 527.

[25] A. Duncan, E. Eichten and H. Thacker, *Electromagnetic splittings and light quark masses in lattice QCD*, *Phys. Rev. Lett.* **76** (1996) 3894 [hep-lat/9602005].

[26] M.G. Endres, A. Shindler, B.C. Tiburzi and A. Walker-Loud, *Massive photons: an infrared regularization scheme for lattice QCD+QED*, *Phys. Rev. Lett.* **117** (2016) 072002 [1507.08916].

[27] A. Patella, *QED Corrections to Hadronic Observables*, *PoS* **LATTICE2016** (2017) 020 [1702.03857].

[28] F. Bloch and A. Nordsieck, *Note on the Radiation Field of the electron*, *Phys. Rev.* **52** (1937) 54.

[29] D. Giusti, V. Lubicz, G. Martinelli, C.T. Sachrajda, F. Sanfilippo, S. Simula et al., *First lattice calculation of the QED corrections to leptonic decay rates*, *Phys. Rev. Lett.* **120** (2018) 072001 [1711.06537].

[30] J. Gasser, A. Rusetsky and I. Scimemi, *Electromagnetic corrections in hadronic processes*, *Eur. Phys. J.* **C32** (2003) 97 [hep-ph/0305260].

[31] [CalLat 20A] N. Miller et al., *Scale setting the Möbius domain wall fermion on gradient-flowed HISQ action using the omega baryon mass and the gradient-flow scales t_0 and w_0*, *Phys. Rev. D* **103** (2021) 054511 [2011.12166].

[32] [RBC/UKQCD 14B] T. Blum et al., *Domain wall QCD with physical quark masses*, *Phys. Rev.* **D93** (2016) 074505 [1411.7017].

[33] [PACS-CS 08] S. Aoki et al., *2+1 flavor lattice QCD toward the physical point*, *Phys. Rev.* **D79** (2009) 034503 [0807.1661].

[34] [ETM 14] N. Carrasco et al., *Up, down, strange and charm quark masses with N_f = 2+1+1 twisted mass lattice QCD*, *Nucl. Phys.* **B887** (2014) 19 [1403.4504].

[35] [MILC 09A] A. Bazavov et al., *MILC results for light pseudoscalars*, *PoS* **CD09** (2009) 007 [0910.2966].

[36] V. Cirigliano and I. Rosell, *$\pi/K \to e\bar{\nu}_e$ branching ratios to $O(e^2p^4)$ in Chiral Perturbation Theory*, *JHEP* **10** (2007) 005 [0707.4464].

[37] B. Ananthanarayan and B. Moussallam, *Four-point correlator constraints on electromagnetic chiral parameters and resonance effective Lagrangians*, *JHEP* **06** (2004) 047 [hep-ph/0405206].

[38] V. Cirigliano and H. Neufeld, *A note on isospin violation in $P_{\ell 2}(\gamma)$ decays*, *Phys.Lett.* **B700** (2011) 7 [1102.0563].

[39] [BMW 12A] S. Borsanyi, S. Dürr, Z. Fodor, C. Hoelbling, S.D. Katz et al., *High-precision scale setting in lattice QCD*, *JHEP* **1209** (2012) 010 [1203.4469].

[40] [RBC/UKQCD 10A] Y. Aoki et al., *Continuum limit physics from 2+1 flavor domain wall QCD*, *Phys.Rev.* **D83** (2011) 074508 [1011.0892].

[41] O. Bar, *Chiral perturbation theory and nucleon–pion-state contaminations in lattice QCD*, *Int. J. Mod. Phys. A* **32** (2017) 1730011 [1705.02806].

[42] M. Lüscher, *Properties and uses of the Wilson flow in lattice QCD*, *JHEP* **08** (2010) 071 [1006.4518], [Erratum: *JHEP* **03** (2014) 092].

[43] C.W. Bernard et al., *The static quark potential in three flavor QCD*, *Phys. Rev.* **D62** (2000) 034503 [hep-lat/0002028].

[44] C. Michael, *Adjoint Sources in Lattice Gauge Theory*, *Nucl. Phys.* **B259** (1985) 58.

[45] M. Lüscher and U. Wolff, *How to Calculate the Elastic Scattering Matrix in Two-dimensional Quantum Field Theories by Numerical Simulation*, *Nucl. Phys.* **B339** (1990) 222.

[46] F. Niedermayer, P. Rufenacht and U. Wenger, *Fixed point gauge actions with fat links: Scaling and glueballs*, *Nucl. Phys. B* **597** (2001) 413 [hep-lat/0007007].

[47] M. Della Morte, A. Shindler and R. Sommer, *On lattice actions for static quarks*, *JHEP* **08** (2005) 051 [hep-lat/0506008].

[48] M. Donnellan, F. Knechtli, B. Leder and R. Sommer, *Determination of the Static Potential with Dynamical Fermions*, *Nucl. Phys. B* **849** (2011) 45 [1012.3037].

[49] A. Hasenfratz and F. Knechtli, *Flavor symmetry and the static potential with hypercubic blocking*, *Phys.Rev.* **D64** (2001) 034504 [hep-lat/0103029].

[50] M. Lüscher and P. Weisz, *Perturbative analysis of the gradient flow in non-abelian gauge theories*, *JHEP* **02** (2011) 051 [1101.0963].

[51] A. Deuzeman and U. Wenger, *Gradient flow and scale setting for twisted mass fermions*, *PoS* **LATTICE2012** (2012) 162.

[52] [ETM 15A] A. Abdel-Rehim et al., *Simulating QCD at the physical point with $N_f = 2$ Wilson twisted mass fermions at maximal twist*, *Phys. Rev.* **D95** (2015) 094515 [1507.05068].

[53] [ETM 21] C. Alexandrou et al., *Ratio of kaon and pion leptonic decay constants with $N_f = 2 + 1 + 1$ Wilson-clover twisted-mass fermions*, *Phys. Rev. D* **104** (2021) 074520 [2104.06747].

[54] O. Bär and M. Golterman, *Chiral perturbation theory for gradient flow observables*, *Phys. Rev.* **D89** (2014) 034505 [1312.4999], [Erratum: *Phys. Rev.* **D89** (2014) 099905].

[55] S. Schaefer, *Status and challenges of simulations with dynamical fermions*, *PoS* **LATTICE2012** (2012) 001 [1211.5069].

[56] A. Ramos and S. Sint, *Symanzik improvement of the gradient flow in lattice gauge theories*, *Eur. Phys. J. C* **76** (2016) 15 [1508.05552].

[57] [MILC 13B] A. Bazavov et al., *Symanzik Flow on HISQ Ensembles*, *PoS* **LATTICE2013** (2014) 269 [1311.1474].

[58] A. Cheng, A. Hasenfratz, Y. Liu, G. Petropoulos and D. Schaich, *Improving the continuum limit of gradient flow step scaling*, *JHEP* **05** (2014) 137 [1404.0984].

[59] Z. Fodor, K. Holland, J. Kuti, S. Mondal, D. Nogradi et al., *The lattice gradient flow at tree-level and its improvement*, *JHEP* **1409** (2014) 018 [1406.0827].

[60] [FNAL/MILC 14A] A. Bazavov et al., *Charmed and light pseudoscalar meson decay constants from four-flavor lattice QCD with physical light quarks*, *Phys.Rev.* **D90** (2014) 074509 [1407.3772].

[61] [FNAL/MILC 17] A. Bazavov et al., *B- and D-meson leptonic decay constants from four-flavor lattice QCD*, *Phys. Rev.* **D98** (2018) 074512 [1712.09262].

[62] [MILC 12B] A. Bazavov et al., *Lattice QCD ensembles with four flavors of highly improved staggered quarks*, *Phys.Rev.* **D87** (2013) 054505 [1212.4768].

[63] [HPQCD 11B] R. J. Dowdall et al., *The upsilon spectrum and the determination of the lattice spacing from lattice QCD including charm quarks in the sea*, *Phys.Rev.* **D85** (2012) 054509 [1110.6887].

[64] [HPQCD 09B] C. T. H. Davies, E. Follana, I. Kendall, G.P. Lepage and C. McNeile, *Precise determination of the lattice spacing in full lattice QCD*, *Phys.Rev.* **D81** (2010) 034506 [0910.1229].

[65] [HPQCD 05B] A. Gray et al., *The upsilon spectrum and m_b from full lattice QCD*, *Phys.Rev.* **D72** (2005) 094507 [hep-lat/0507013].

[66] [ETM 20] G. Bergner, P. Dimopoulos, J. Finkenrath, E. Fiorenza, R. Frezzotti, M. Garofalo et al., *Quark masses and decay constants in $N_f = 2 + 1 + 1$ isoQCD with Wilson clover twisted mass fermions*, in *37th International Symposium on Lattice Field Theory (Lattice 2019) Wuhan, Hubei, China, June 16-22, 2019*, vol. LATTICE2019, p. 181, 2020, DOI [2001.09116].

[67] [MILC 15] A. Bazavov et al., *Gradient flow and scale setting on MILC HISQ ensembles*, *Phys. Rev.* **D93** (2016) 094510 [1503.02769].

[68] [HPQCD 13A] R. Dowdall, C. Davies, G. Lepage and C. McNeile, *V_{us} from π and K decay constants in full lattice QCD with physical u, d, s and c quarks*, *Phys.Rev.* **D88** (2013) 074504 [1303.1670].

[69] [RQCD 22] G. S. Bali, S. Collins, P. Georg, D. Jenkins, P. Korcyl, A. Schäfer et al., *Scale setting and the light baryon spectrum in $N_f = 2 + 1$ QCD with Wilson fermions*, 2211.03744.

[70] [CLS 21] B. Strassberger et al., *Scale setting for CLS 2+1 simulations*, *PoS* **LATTICE2021** (2022) 135 [2112.06696].

[71] [CLS 16] M. Bruno, T. Korzec and S. Schaefer, *Setting the scale for the CLS 2+1 flavor ensembles*, *Phys. Rev.* **D95** (2017) 074504 [1608.08900].

[72] [QCDSF/UKQCD 15B] V. .G. Bornyakov et al., *Wilson flow and scale setting from lattice QCD*, 1508.05916.

[73] [HotQCD 14] A. Bazavov et al., *Equation of state in (2+1)-flavor QCD*, *Phys.Rev.* **D90** (2014) 094503 [1407.6387].

[74] V. Bornyakov et al., *Determining the scale in Lattice QCD*, 12, 2015 [1512.05745].

[75] [HotQCD 11] A. Bazavov, T. Bhattacharya, M. Cheng, C. DeTar, H. Ding et al., *The chiral and deconfinement aspects of the QCD transition*, *Phys.Rev.* **D85** (2012) 054503 [1111.1710].

[76] [MILC 10] A. Bazavov et al., *Results for light pseudoscalar mesons*, *PoS* **LAT2010** (2010) 074 [1012.0868].

[77] [χQCD 14] Y. Yi-Bo et al., *Charm and strange quark masses and f_D_s from overlap fermions*, *Phys. Rev.* **D92** (2015) 034517 [1410.3343].

[78] [MILC 09] A. Bazavov et al., *Full nonperturbative QCD simulations with 2+1 flavors of improved staggered quarks*, *Rev. Mod. Phys.* **82** (2010) 1349 [0903.3598].

[79] C. Aubin et al., *Light hadrons with improved staggered quarks: Approaching the continuum limit*, *Phys. Rev.* **D70** (2004) 094505 [hep-lat/0402030].

[80] [MILC 09B] A. Bazavov et al., *Results from the MILC collaboration's SU(3) chiral perturbation theory analysis*, *PoS* **LAT2009** (2009) 079 [0910.3618].

[81] [HPQCD 03] M. Wingate, C.T. Davies, A. Gray, G.P. Lepage and J. Shigemitsu, *The B_s and D_s decay constants in three flavor lattice QCD*, *Phys.Rev.Lett.* **92** (2004) 162001 [hep-ph/0311130].

[82] [ALPHA 14A] M. Bruno, J. Finkenrath, F. Knechtli, B. Leder and R. Sommer, *Effects of Heavy Sea Quarks at Low Energies*, *Phys. Rev. Lett.* **114** (2015) 102001 [1410.8374].

[83] [ALPHA 17A] F. Knechtli, T. Korzec, B. Leder and G. Moir, *Power corrections from decoupling of the charm quark*, *Phys. Lett. B* **774** (2017) 649 [1706.04982].

[84] [ALPHA 20] R. Höllwieser, F. Knechtli and T. Korzec, *Scale setting for $N_f = 3+1$ QCD*, *Eur. Phys. J. C* **80** (2020) 349 [2002.02866].